The Synergy between a Silver-Ruthenium Antimicrobial and aminoglycosides is based on severe macromolecular damage

Emmanuel P. Oladokun[1], Gracious Y. Donkor[1], Julius K. Narh[1], Grady D. Jakobson[1], Cade Ward[1], Patrick O. Tawiah[1], Lisa K. Polzer[1], Kevin A. Edwards[1], Kyle A. Floyd[1], and Jan-Ulrik Dahl[1;*]

[1] School of Biological Sciences, Illinois State University, Normal, IL

Running Title: Reactive oxygen species in antimicrobial therapy

*Address correspondence to Dr. Jan-Ulrik Dahl, School of Biological Sciences, Illinois State University, Campus Box 4120, Normal, IL 61790, phone: (309) 438-7694, email: jdahl1@ilstu.edu

Word Count:

Abstract: 207

Manuscript:

ABSTRACT

The rise of multidrug-resistant (MDR) bacterial pathogens, including uropathogenic *Escherichia coli* (UPEC), highlights the urgent need for alternative treatment strategies to restore antibiotic efficacy. The silver-ruthenium antimicrobial AGXX® exerts potent bactericidal effects through the production of reactive oxygen species (ROS), however, its potential synergy with antibiotics has not been thoroughly investigated. Here, we show that sublethal concentrations of AGXX® strongly enhance aminoglycoside-mediated killing across a diverse panel of Gram-negative and Gram-positive MDR clinical isolates, including highly aminoglycoside-resistant strains. Combinational treatments significantly reduced the effective concentrations of gentamicin, tobramycin, kanamycin, and amikacin required for bacterial killing. Mechanistic analyses revealed that AGXX®/aminoglycoside co-treatment induces a pronounced intracellular ROS accumulation, leading to severe proteotoxic stress, extensive protein aggregation, and DNA damage. Scavenging ROS abolished synergistic killing, establishing oxidative imbalance as the primary driver of the synergy between both antimicrobials. We further identify polyphosphate as a key bacterial defense mechanism that mitigates ROS accumulation, proteotoxicity, and genotoxic stress during combinational treatment. Moreover, AGXX®–aminoglycoside synergy was preserved in artificial urine medium and across clinical UPEC isolates, underscoring the relevance for urinary tract infections. Together, these findings position AGXX® as a potent aminoglycoside adjuvant that restores antibiotic efficacy through ROS-driven macromolecular damage, supporting its development for combination therapies against MDR bacterial infections.

INTRODUCTION

Originally isolated from *Streptomyces spp.* and *Micromonaspora*, respectively, aminoglycoside antibiotics have now also been developed as semisynthetic derivates (1). These bactericidal antimicrobials are polycationic and enter bacteria in three steps. Firstly, ionic interactions are established between the polycationic moieties of aminoglycosides and negatively charged components of the cell surface, including those found in lipopolysaccharide (LPS) (2, 3), displace divalent cations from aminoglycoside binding sites. This, in turn, results in the destabilization of LPS components and the disruption of outer membrane integrity in an energy-independent way (4). Driven by an increased proton motif force particularly in aerobically respiring bacteria,

59 aminoglycosides cross the plasma membrane and enter the cytoplasm, where they bind to the
60 aminoacyl-tRNA recognition site and interact with the 16S ribosomal RNA, ultimately causing
61 protein mistranslation that can lead to protein misfolding [recently reviewed in (1)]. Misfolded
62 proteins can be inserted into the plasma membrane and form irregular membrane channels that
63 further exacerbate aminoglycoside uptake, and subsequent bactericidal effects (5, 6). Although
64 controversial (7), ROS production caused by the hyperactivation of the electron transport chain in
65 aerobically respiring bacteria has been proposed as a potential contributor to the bactericidal nature
66 of aminoglycosides (5, 6, 8). Likewise, aminoglycoside resistance observed in most anaerobic
67 bacteria could be explained by a lack in sufficiently high proton motive force that aminoglycoside
68 uptake depends on (5, 9). Moreover, Ezraty *et al.* showed that iron-sulfur cluster-containing
69 proteins play an important factor for aminoglycoside uptake, ultimately contributing to the
70 bactericidal effects of these antibiotics (10).
71
72 Resistance to aminoglycosides has now been reported in all ESKAPEE pathogens, including the
73 Gram-negative bacterium *Escherichia coli*. *E. coli* colonizes the gastrointestinal (GI) tract of
74 human newborns shortly after birth, where they establish themselves as part of the commensal gut
75 microbiome. Beyond commensal symbiosis, additional *E. coli* serotypes can be pathogenic
76 resulting in life-threatening diarrheal disease, including enteropathogenic, enterohemorrhagic,
77 enterotoxigenic, enteroinvasive, enteroaggregative, and diffusely adherent *E. coli* serotypes (11).
78 Moreover, extraintestinal pathogenic *E. coli* serotypes (ExPEC) can often still colonize the GI tract
79 and serve commensal functions. It is only after dissemination from the GI tract and entry into their
80 primary site of infection, that ExPEC strains become pathogenic. The most common ExPEC
81 serotype is uropathogenic *E. coli* (UPEC), the etiologic agent of most urinary tract infections
82 (UTIs) (11). UPEC traverse the urethra to establish infection within the bladder (cystitis) and can
83 further ascend the ureters to cause infection within the kidneys (pyelonephritis), which if left
84 untreated can result in the development of potentially life-threatening septicemia (12, 13). UTIs
85 account for approximately 20% – 50% of all nosocomial infections (14), many of which occur in
86 catharized patients. Biofilm formation on in-dwelling urinary catheters is the main driving force
87 behind catheter-associated UTIs (CAUTIs), and serves as a reservoir for continued seeding of
88 infection within the urinary tract (12, 13, 15). There is also increasing evidence for the presence
89 of antimicrobial resistance (AMR) related genes within UPEC (16). The inherent infection

90 mechanisms of UPEC, the ability to form catheter-associated biofilms, and the rise in prevalence
91 of AMR highlight the urgent need for the development of improved antimicrobial compounds and
92 catheter surface-coatings to treat or prevent UTI (17, 18).
93
94 Despite its long-standing history and high efficacy against bacteria, the antimicrobial mode of
95 action of silver (Ag) remains poorly understood, although changes in DNA condensation,
96 membrane alteration, and protein damage have been associated with Ag (19). Ag^+ ions can
97 indirectly damage protein through interaction with cysteine thiols, destabilization of iron-sulfur
98 clusters, replacement of metal-containing cofactors, and through promotion of reactive oxygen
99 species (ROS) generation (19). Over the last two decades, silver derivates have received increased
100 attention for use as antimicrobial surface-coatings that can protect from biofilm-forming bacteria
101 and reduce the risk of nosocomial infections (20). One such silver-containing surface coating is
102 AGXX® (21, 22). All AGXX® formulations consist of a silver-ruthenium complex, but differ in
103 the silver-ruthenium ratio, particle size, and production procedure which may affect their
104 antimicrobial activity (23, 24). AGXX® has been shown to be more potent than silver alone,
105 inhibiting the growth of a range of pathogenic bacteria by eliciting a thiol-specific oxidative stress
106 response (22, 25–27). We recently reported that AGXX® potentiates the efficacy of
107 aminoglycoside antibiotics, when used in combination, against the opportunistic pathogen
108 *Pseudomonas aeruginosa* (26). The synergistic bactericidal effects against *P. aeruginosa* are
109 mediated by elevated ROS levels in the cells, which disrupt Fe/S-clusters in metabolic enzymes,
110 lead to elevated free iron, trigger hydroxyl radical formation, and result in a significant increase in
111 outer and inner membrane permeability to exacerbate aminoglycoside influx into the cell (26).
112
113 In this current study, we provide novel information on the cellular consequences of the synergy
114 between AGXX® and aminoglycosides in a variety of Gram-positive and Gram-negative
115 pathogens, including UPEC and highly aminoglycoside-resistant clinical isolates of various
116 ESKAPEE pathogens. This synergy appears to primarily rely on the generation of ROS, as co-
117 supplementation with an antioxidant abolishes AGXX®/aminoglycoside-induced cell death. For
118 the first time, we provide direct evidence that AGXX®/aminoglycoside co-treatments promote
119 extensive protein aggregation and induce DNA damage. However, despite the potent toxicity of
120 AGXX®/aminoglycoside co-treatment, we found that UPEC can activate sophisticated defenses

121 by expressing molecular chaperones such as IbpA and producing the chemical chaperone
122 polyphosphate (polyP). We observed that the presence of polyP reduces intracellular ROS
123 accumulation to decrease DNA damage and protein aggregation and positively affects UPEC
124 survival underscoring the significant role of polyP in oxidative stress defense.
125

126 **RESULTS**

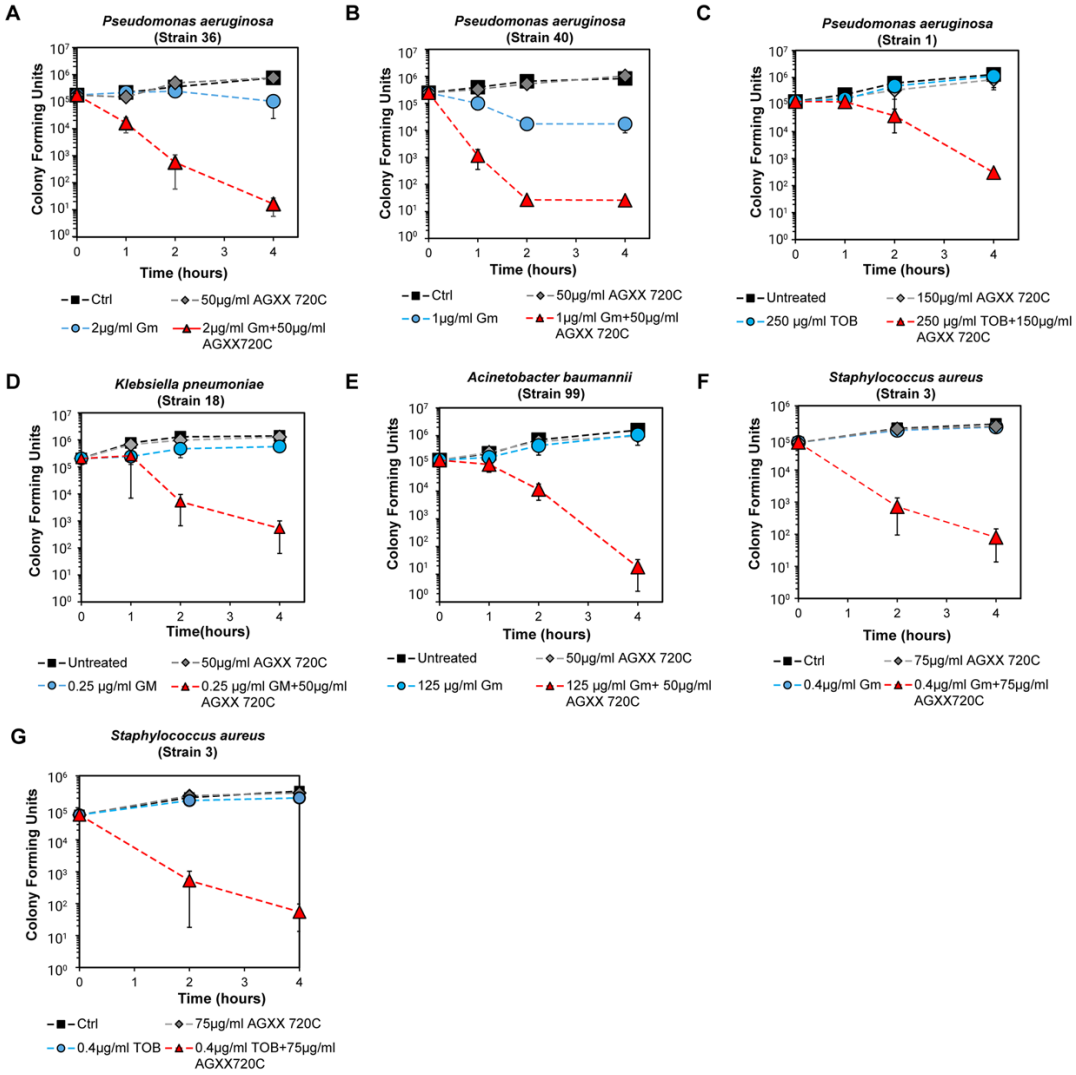

127

128 **Fig. 1: AGXX enhances the bactericidal effects of aminoglycoside antibiotics in various**
129 **multidrug-resistant ESKAPEE pathogens.** Time-killing survival studies were performed on
130 various clinical isolates of *P. aeruginosa* (**A–C**), *K. pneumoniae* (**D**), *A. baumannii* (**E**), and *S.*
131 *aureus* (**F, G**). Mid-log phase cells were exposed to sublethal concentrations of gentamycin (Gm),
132 tobramycin (TOB), AGXX®720C, or combinations as indicated. Bacterial survival was quantified
133 by determining colony-forming units (CFUs) at the indicated time points post-treatment (0–4 h).
134 (n = 3, ±SD).

135 **AGXX enhances the bactericidal effects of aminoglycoside antibiotics in various multidrug-**
136 **resistant pathogens.** The rapid emergence of multidrug-resistant pathogens (MDR) requires
137 alternative treatment options, such as the development of therapies to increase the effectiveness of
138 existing antibiotics. The silver-ruthenium antimicrobial AGXX®, which was shown to be effective
139 against laboratory strains of both Gram-positive and Gram-negative pathogens (22–25, 27, 28),
140 may provide such opportunity. As previously reported by us, AGXX® potentiates the activity of
141 aminoglycoside antibiotics in the laboratory *P. aeruginosa* strain PA14, which is due to elevated
142 aminoglycoside uptake as a result of ROS-induced membrane damage (26). To exclude any strain-
143 specific effects and assess the effectiveness of AGXX®/aminoglycoside combinations on other
144 bacterial pathogens, we examined the impact of AGXX®/aminoglycosides against a panel of
145 Gram-negative and Gram-positive clinical isolates obtained from burn wound patients. With
146 minimal inhibitory concentrations (MIC) between 1 and >2,000 μg/ml, these isolates differ quite
147 significantly in their susceptibility to gentamycin (Gm) and tobramycin (Tob), respectively
148 (**Supplementary Table S1**). We exposed *P. aeruginosa* strains 1, 36, and 40, *Klebsiella*
149 *pneumoniae* strain 18, *Acinetobacter baumannii* strain 99, and *Staphylococcus aureus* strain 3 to
150 the indicated sublethal concentrations of AGXX®720C, aminoglycosides, or their combination
151 and monitored bacterial survival over 4 hours by enumerating colony-forming units (CFUs).
152 Individual treatments with sublethal concentrations of AGXX®720C or aminoglycoside had
153 minimal (*P. aeruginosa* strains 36 and 40) to no bactericidal effects across these strains (**Fig. 1A–**
154 **G**). In contrast, combinational treatments with AGXX®720C and aminoglycosides resulted in
155 rapid synergistic killing, with ~3-log or greater reductions in CFUs observed in all tested strains
156 after 4 hours. This effect was particularly pronounced against *P. aeruginosa* strain 1 and *A.*
157 *baumannii* strain 99, which both have Gm/Tob MICs >500 μg/ml (**Supplementary Table S1**).
158 Notably, sub-MIC concentrations of Gm/Tob combined with AGXX®720C significantly reduced
159 their survival by over 3-log, thus rendering these highly resistant isolates sensitive to
160 aminoglycosides again (**Fig. 1C, 1E**). These findings demonstrate the therapeutic promise of
161 AGXX® as a broad-spectrum compound capable of enhancing aminoglycoside activity against
162 both Gram-negative and Gram-positive MDR pathogens.

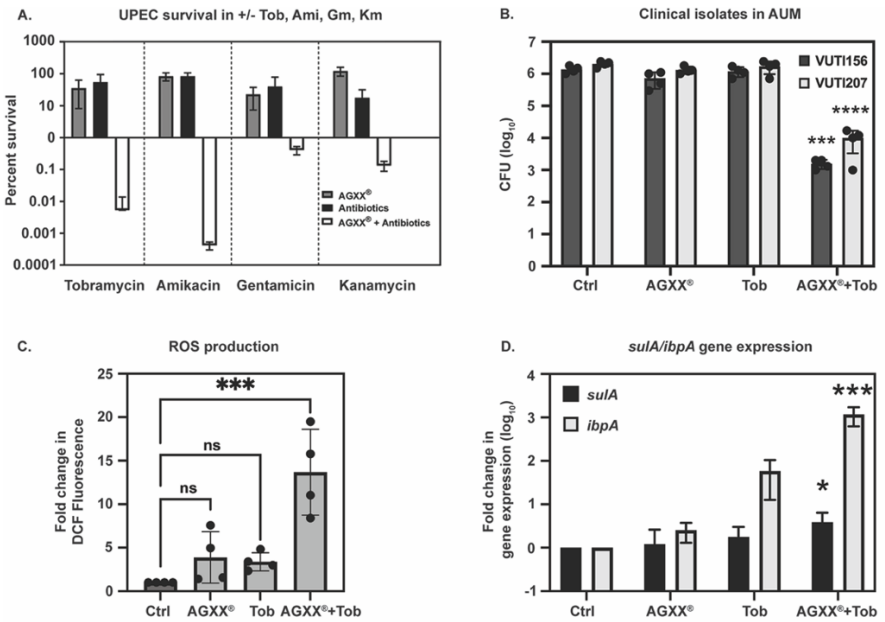

Fig. 2. AGXX®/aminoglycoside co-treatment causes severe oxidative stress and elicits stress responses in UPEC. (A) Exponentially growing cells of UPEC strain CFT073 was exposed to sublethal concentrations of tobramycin (Tob, 0.75 µg/mL), amikacin (Ami, 0.875 µg/mL), gentamicin (Gm, 0.01 µg/mL), kanamycin (Kan, 1 µg/mL), or AGXX®394C (30 µg/mL), individually and in combination. CFU counts were determined after 3 hours of incubation. The % survival, normalized to untreated CFUs, is plotted (n = 3-4, ±SD). **(B)** UPEC clinical isolates VUTI207 and VUTI156 were grown in artificial urine media (AUM) and treated with 1 µg/mL Tob or 30 µg/mL AGXX®394C individually and in combination. CFU counts were determined after 3 hours of incubation (n = 4, ±SD; statistical analysis: one-way ANOVA, Dunnett's posttest, *** $P < 0.001$, **** $P < 0.0001$). (**C-D**) Mid-log phase CFT073 cells were treated with sublethal concentrations of Tob (0.5 µg/mL) or AGXX®394C (30 µg/mL) individually and in combination. **(C)** ROS levels were measured by H_2DCFDA fluorescence (n = 4, ±SD, statistical analysis: one-way ANOVA, Dunnett's posttest, ns = $P > 0.05$, *** $P < 0.001$). (**D**) *ibpA* and *sulA* transcript levels were determined by qRT-PCR. Expression of each gene was normalized to the housekeeping gene *rrsD* and calculated as fold change relative to untreated cells (n = 4, ±SD; statistical analysis: one-way ANOVA, Dunnett's posttest, * $P < 0.05$, *** $P < 0.001$).

AGXX®/aminoglycoside co-treatment causes severe oxidative stress in uropathogenic *E. coli* (UPEC). Silver and silver-containing compounds have become increasingly popular as surface-coatings on medical devices, such as catheters, to prevent bacterial attachment and reduce the risk of developing CAUTIs, a significant health problem for hospitalized patients and those living in long-term care facilities (15). The most prominent causative agent of CAUTIs is UPEC, which readily adheres to catheters and forms stress-/treatment-resistant biofilms. To examine the efficacy of AGXX®/aminoglycoside combinational treatment of UPEC, we treated mid-log phase CFT073 cells with sublethal concentrations of Tob, amikacin (Ami), Gm, or kanamycin (Kan), alone and

189 in combination with 30 µg/mL of a more recent AGXX formulation (*i.e.* AGXX®394C), and
190 quantified bacterial survival via CFU enumeration after 60 minutes. Individual treatments of
191 AGXX®394C and the four aminoglycosides had minimal effects on CFT073, only reducing
192 survival by less than 1-log (**Fig. 2A**). However, combination treatment of AGXX®394C and any
193 aminoglycoside (most notably Tob and Ami), decreased CFT073 survival by up to 4-logs (**Fig.**
194 **2A**). A similar synergistic effect was observed for AGXX®394C/Tob treatment of two UPEC
195 clinical isolates VUTI156 (pyelonephritis) and VUTI207 (cystitis), which further demonstrates
196 combinatorial effects with clinically relevant UPEC isolates (**Fig. 2B**). These experiments were
197 conducted in artificial urine media (AUM), to more closely mimic conditions found within the
198 urinary tract (29). Next, we sought to characterize the strength of the synergistic interaction
199 between AGXX® and aminoglycosides in CFT073. We performed a checkerboard assay using
200 varying concentrations of the Gm, Kan, Ami, and Tob in the presence or absence of 30 µg/mL
201 AGXX®720C. We observed that the addition of AGXX®720C decreased the aminoglycoside
202 concentrations required for complete growth inhibition by 16.7-fold for Gm, 3-fold for Kan, 4-
203 fold for Ami, and 3.8-fold for Tob (**Supplementary Figure S1**), indicating that AGXX®,
204 regardless of its formulation, potentiates aminoglycoside antibiotics.
205
206 In *P. aeruginosa*, we previously showed that the synergistic effects between AGXX® and sub-
207 lethal aminoglycoside concentrations is attributed to increased accumulation of ROS (26). We
208 observed a similar ROS accumulation in UPEC strain CFT073, where neither AGXX®394C nor
209 Tob alone increased ROS levels, but AGXX®394C co-treatment with a sub-lethal Tob
210 concentration resulted in a ~13-fold increase in ROS levels relative to untreated controls (**Fig. 2C**).
211 Increased ROS levels pose a risk to cellular macromolecules, especially proteins and nucleic acids
212 (30, 31). However, bacteria have evolved intricate systems to deal with the negative consequences
213 of ROS, and eliminate ROS-mediated damage, including through transcriptional up-regulation of
214 heat-shock and SOS responses (32–36). To determine if AGXX®394C/Tob co-treatment elicits
215 increased responses indicative of macromolecular damage, we examined the transcript levels of
216 hallmark genes for protein aggregation (*i.e. ibpA*) and DNA damage (*i.e. sulA*) using qRT-PCR.
217 Expression of *ibpA*, encoding a small heat shock protein that protects against proteotoxic stress
218 (37), was induced 2.5-fold and 58-fold by individual exposure to AGXX®394C or Tob,
219 respectively, while no significant change in expression of the gene *sulA*, a gene encoding for the

220 SOS cell division inhibitor activated during DNA damage (38), was observed with individual
221 treatments (**Fig. 2D**). However, AGXX®394C/Tob co-treatment resulted in over 1,000-fold
222 increase in *ibpA* and a 5-fold increase in *sulA* expression (**Fig. 2D**), suggesting that the synergy
223 between AGXX® and aminoglycosides in CFT073 may be based on a more pronounced
224 macromolecular damage.
225

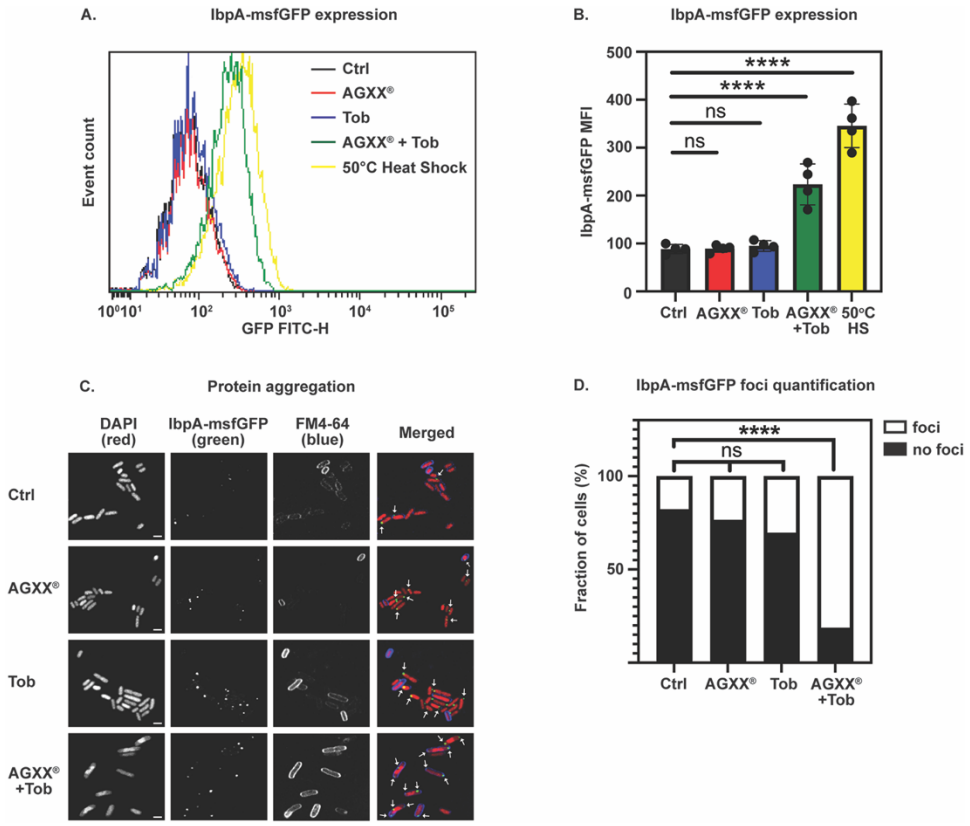

226

227 **Fig. 3. The synergy between AGXX® and aminoglycosides is due to increased proteotoxic**
228 **effects, evoking elevated expression of molecular chaperones**. Cellular IbpA-msfGFP
229 fluorescence was quantified after 1 hour of exposure of mid-log phase *E. coli* cells to sublethal
230 concentrations of AGXX®394C (15 µg/mL), Tob (0.3 µg/mL) or their combination. Untreated
231 cells serve as the negative control and 50°C heat shocked cells as the positive control. (**A**) Total
232 cellular IbpA-msfGFP fluorescence determined by flow cytometry. One representative dataset of
233 four biological replicates is shown. (**B**) Quantification of mean fluorescence intensity (MFI) of
234 IbpA-msfGFP fluorescence determined by flow cytometry (n = 4, ±SD; statistics: One-way
235 ANOVA, Dunnett's multiple comparison test, ns = P > 0.05, ****P < 0.0001)). (**C**) For
236 visualization and quantification of protein aggregates *in vivo*, cells were stained with DAPI (to
237 visualize nucleic acids, red) and FM4-64 (to visualize membranes, blue). White arrows indicate
238 foci formed by IbpA-msfGFP (green) binding to protein aggregates *in vivo*. Images representative
239 of three biological replicates. (**D**) Quantification of the number of foci per cell from microscopy
240 images as shown in **(C)** (n=3, ±SD; statistics: Tukey's multiple comparison test, ns = P > 0.05,
241 ****P < 0.0001).

242 **The synergy between AGXX® and aminoglycosides is due to increased proteotoxic effects,**
243 **evoking elevated expression of molecular chaperones.** Following up on our transcriptional data
244 pointing towards increased macromolecular damage in bacteria treated with AGXX®394C/Tob
245 combinations, we assessed the extent of protein aggregate formation *in vivo* in the presence and
246 absence of individual or combined treatments with sublethal AGXX®394C and/or Tob
247 concentrations. We utilized a reporter strain harboring a chromosomal fusion between *ibpA* and
248 monomeric super folder green fluorescent protein under the control of the native *ibpA* promoter.
249 IbpA expression is induced under stress conditions that induce protein unfolding (39), and IbpA-
250 msfGFP has been used previously to monitor and quantify protein aggregation *in vivo* (27, 40).
251 We exposed *E. coli* cells expressing IbpA-msfGFP to sublethal concentrations of AGXX®394C
252 (15 µg/mL), Tob (0.3 µg/mL), or their combination for one hour, and measured IbpA-msfGFP
253 fluorescence via flow cytometry. As a positive control, we induced protein aggregation through
254 heat-shock by exposing cells to 50 ˚C for 60 mins, which resulted in the most pronounced IbpA-
255 msfGFP fluorescence (**Supplementary Fig. S2**). The combination treatment of AGXX®394C and
256 Tob induced a pronounced shift in fluorescence intensity representing an ~2-fold increase in IbpA-
257 msfGFP fluorescence **(Fig. 3A-B)**, comparable to the 50°C heat-shock control, while there was no
258 significant change in IbpA-msfGFP fluorescence observed for the individual treatments and
259 untreated controls **(Fig. 3A-B)**. Visualization of IbpA-msfGFP fluorescent foci by confocal
260 microscopy, showed a similar trend for cells exposed to either individual or combined treatments
261 for 60 minutes (**Fig. 3C-D**). Approximately 25% and 30% of cells showed a single IbpA-sfGFP
262 foci per cell upon individual treatment with AGXX®394C or Tob, respectively, which is
263 comparable to the 20% of cells with a foci observed for in untreated cells (**Fig. 3C-D**). However,
264 IbpA-sfGFP foci formation was significantly higher upon AGXX®394C/Tob combinational
265 treatment, where 85% of cells had foci, and approximately 30% of those cells harbored multiple
266 foci per cell (**Fig. 3C-D**). Overall, our results provide direct evidence for increased proteotoxicity
267 as the result of the synergy between AGXX®394C and Tob.
268

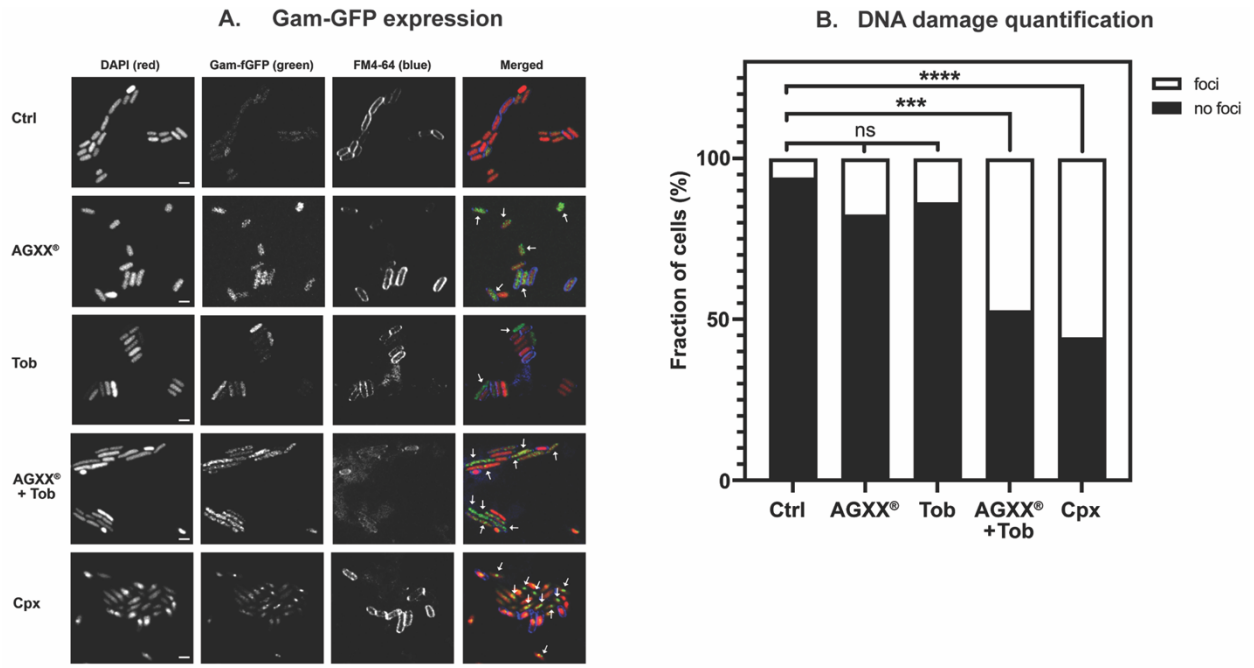

Fig. 4. The AGXX® and aminoglycoside synergy exacerbates DNA damage. (**A, B**) Exponentially growing *E. coli* cells expressing Gam-sfGFP were treated with sub-lethal concentrations of AGXX®394C (15 µg/mL), Tob (0.3 µg/mL), or a combination thereof for 3 hours. Untreated cells serve as the negative control and treatment with 20 µg/ml ciprofloxacin (Cpx) as the positive control. Samples were stained with DAPI (red) and FM4-64 (blue). Confocal images were analyzed by blind-counting Gam-sfGFP (green) foci. (**A**) Arrows indicate Gam-sfGFP foci representing sites of DNA damage. Images representative of three biological replicates. (**B**) Quantification of the number of foci per cell from microscopy images as shown in **(A)** (n=3; ±SD; statistics: Two-way ANOVA, Tukey's multiple comparison test, ns = $P > 0.05$, ***$P < 0.001$, ****$P < 0.0001$).

The AGXX® and aminoglycoside synergy exacerbates DNA damage. While our qRT-PCR analysis revealed the transcriptional upregulation of *sulA* in response to AGXX®394C/Tob co-treatment (**Fig. 2D**), we next sought to further determine if co-treatment induces significant DNA damage. To monitor and quantify DNA damage, we used *E. coli* cells that overexpress the bacteriophage protein Gam fused to GFP. Gam-sfGFP has been previously shown to specifically bind to DNA double-strand breaks in both bacterial and mammalian cells (41). Gam-sfGFP expression was induced by addition of doxycycline in cells either left untreated or treated with AGXX®394C and Tob individually or in combination. Only ~15% and ~18% of cells treated with Tob and AGXX®394C showed one detectable Gam-sfGFP foci respectively, which did not differ significantly from the ~5% observed in untreated cells (**Fig. 4A-B**). Combinational AGXX®394C/Tob treatment induced a significant increase in Gam-sfGFP foci, with ~50% of

292 cells having at least one foci, which was comparable to the positive control treatment with
293 ciprofloxacin, a DNA-damaging fluoroquinolone (**Fig. 4A-B**).
294

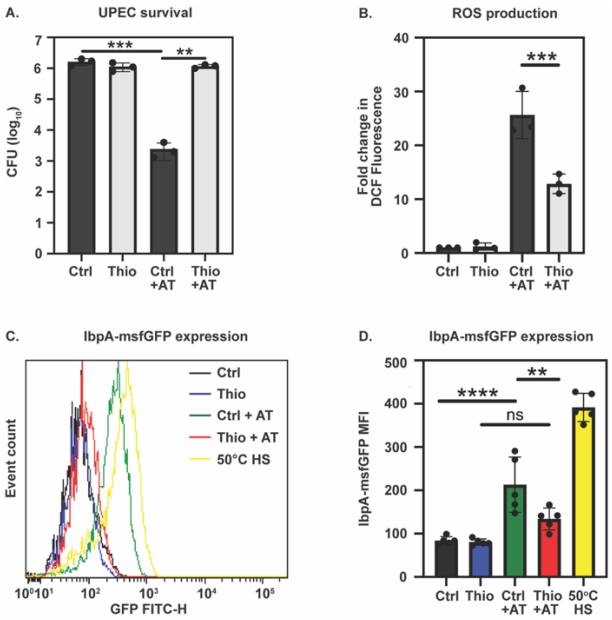

295

296 **Fig. 5. The ROS-mediated synergistic effects between AGXX® and Tob can be suppressed**
297 **by antioxidants.** (**A, B**) Exponentially growing CFT073 cells were exposed for 60 minutes to a
298 combination of AGXX®394C (30 µg/mL) and Tob (0.5 µg/mL), labelled as "AT". Cells left
299 untreated served as control. Prior to reaching mid-log phase, cells were either left untreated or
300 pretreated with 70 mM thiourea before subsequent exposure to the stress treatment. (**A**) Bacterial
301 survival was assessed by determining CFUs after 1 hour of treatment. (n = 3, ±SD; statistics: one-
302 way ANOVA, Dunnett's posttest; ** $P < 0.01$, *** $P < 0.001$). (**B**) Intracellular ROS levels were
303 quantified using H2DCFDA fluorescence. (n = 3, ±SD; statistics: one-way ANOVA, Dunnett's
304 posttest; *** $P < 0.001$). (**C, D**) For IbpA-sfGFP expression analysis via flow cytometry, mid-log
305 phase cells were exposed for 60 minutes to either a combination of AGXX394C (15 µg/mL) and
306 Tob (0.3 µg/mL) (AT), left untreated, or subjected to a heat-shock at 50°C as a positive control.
307 (**C**) Total cellular IbpA-msfGFP fluorescence determined by flow cytometry. One representative
308 dataset of four biological replicates is shown. (**D**) Quantification of mean fluorescence intensity
309 (MFI) of IbpA-msfGFP fluorescence determined by flow cytometry (n = 4, ±SD; statistics: one-
310 way ANOVA, Dunnett's posttest; ns = $P > 0.05$, ** $P < 0.01$, **** $P < 0.0001$).
311

312 **The ROS-mediated effects generated by AGXX® and Tob synergy can be suppressed by**
313 **antioxidants.** Our data suggests that the increased sensitivity of UPEC to the synergy between
314 AGXX® and aminoglycosides results from augmented intracellular ROS accumulation, which
315 promotes protein aggregation and DNA damage. It has previously been proposed that the
316 bactericidal effects of aminoglycoside antibiotics are at least in part due to induction of protein
317 misfolding, and insertion of misfolded proteins into the plasma membrane to create membrane

318 channels and uncontrolled drug uptake (6, 42). To this end, we examined whether a known ROS
319 scavenger, thiourea, mitigates the cellular stress induced by AGXX®/aminoglycoside combined
320 treatment. To test this, CFT073 cultures were pretreated with thiourea (or left untreated) prior to
321 exposure AGXX®394C/Tob co-treatment, and bacterial survival and intracellular ROS levels
322 were determined. As expected, in the absence of thiourea, cells subjected to the combined
323 treatment exhibited a ~3-log reduction in survival (**Fig. 5A**) and a ~25-fold increase in ROS
324 production (**Fig. 5B**). Thiourea pretreatment restored bacterial survival almost completely, and
325 significantly reduced ROS levels by ~50% (**Fig. 5A-B**). Furthermore, pretreatment with thiourea
326 also mitigated the induction of IbpA-msfGFP fluorescence to levels observed under unstressed
327 conditions (**Fig. 5C-D**). These findings further suggest that ROS production is a key contributor
328 to the bactericidal effects of the AGXX®/aminoglycoside combinational treatment.
329

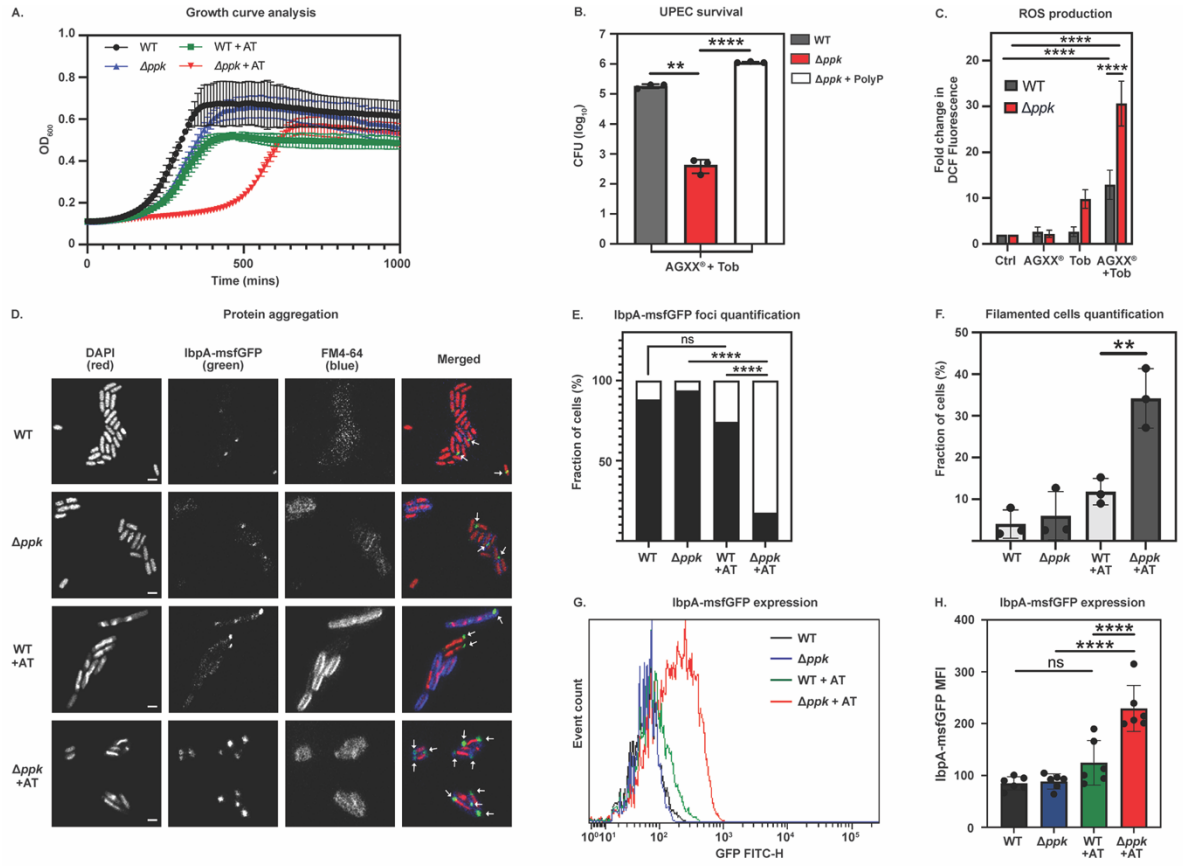

330

331 **Fig. 6. PolyP protects UPEC from AGXX®/aminoglycoside-mediated proteotoxicity.** (**A**)
332 UPEC strains CFT073 and CFT073Δ*ppk* were treated with a combination of AGXX®394C (0.4
333 µg/mL) and Tob (0.2 µg/mL). Growth was monitored over 18 hours. (n = 3, ±SD). (**B, C**) The
334 indicated strains were treated with a combination of AGXX®394C (30 µg/mL) and Tob (0.5

335 μg/mL) for 60 minutes. (**B**) Survival rate as determined by CFU counts (n = 3, ±SD; statistics:
336 two-way ANOVA with Tukey's multiple comparison test: **P < 0.01, ****P < 0.0001). (**C**)
337 Intracellular ROS levels were quantified using H2DCFDA fluorescence; two-way ANOVA with
338 Tukey's multiple comparison test: ****P < 0.0001). (**D-F**) Exponentially growing WT and Δ*ppk*
339 cells expressing IbpA-msfGFP were left untreated or treated with a combination of AGXX®394C
340 (10 μg/mL) and Tob (0.2 μg/mL) for 1 hour. (**D**) For visualization and quantification of protein
341 aggregates *in vivo*, cells were stained with DAPI (red) and FM4-64 (blue). White arrows indicate
342 foci formed by IbpA-msfGFP (green) binding to protein aggregates *in vivo*. Images representative
343 of three biological replicates. **(E)** Quantification of the number of foci per cell from three biological
344 replicates (n=3, ±SD; statistics: two-way ANOVA with Tukey's multiple comparison test, ns = P
345 > 0.05, ****P < 0.0001). **(F**) Quantification of the number of filamentous cells observed in
346 microscopy images as represented in **(D)** (n=3, ±SD; statistics: two-way ANOVA with Tukey's
347 multiple comparison test, **P < 0.01). (**G, H**) Total cellular IbpA-msfGFP fluorescence was
348 determined by flow cytometry. (**G**) A representative image from six biological replicates is shown.
349 (**H**) Quantification of mean fluorescence intensity (MFI) of IbpA-msfGFP fluorescence
350 determined by flow cytometry (n = 6, ±SD; statistics: one-way ANOVA, Dunnett's posttest; ns =
351 P > 0.05, **** P < 0.0001).
352
353

354 **Polyphosphate protects UPEC from AGXX®/aminoglycoside co-treatment induced**
355 **proteotoxicity.** In addition to activating protein-based molecular chaperones like IbpA, many
356 Gram-negative pathogens can also respond to proteotoxic antimicrobials by converting cellular
357 ATP into polyphosphate (polyP), a chemical chaperone that aids in preventing protein aggregation
358 (43, 44). We have recently shown that UPEC cells lacking the enzyme for polyP production (i.e.
359 Δ*ppk*) are more susceptible to AGXX® (27). To test whether polyP protects CFT073 from the
360 proteotoxic effects AGXX/Tob co-treatment, we analyzed its ability to grow and survive with and
361 without polyP kinase Ppk1 upon exposure to the combination of AGXX®394C/Tob. A growth
362 comparison of AGXX®394C/Tob-treated WT and Δ*ppk* cells showed a significantly longer lag
363 phase of polyP-deficient cells (**Fig. 6A**). Notably, when keeping the concentration of one stressor
364 constant while varying the concentration of the other, it became apparent that polyP protects cells
365 from both AGXX®394C and Tob (**Supplementary Fig. S3**). In our survival studies, we exposed
366 exponentially growing WT and Δ*ppk* cells to AGXX®394C /Tob for 1 hour before the cells were
367 serially diluted for CFU counts. In the absence of Ppk1, AGXX AGXX®394C/Tob co-treatment
368 resulted in a ~2.5-log lower survival compared to the wild-type, indicating an increased sensitivity
369 to AGXX®394C/Tob, which could be fully restored by complementation (**Fig. 6B**). Consistent
370 with these findings, we found that Δ*ppk* cells were also characterized by much higher ROS levels
371 upon treatment with Tob alone and when combined with AGXX®394C (**Fig. 6C**). Next, we sought

372 to analyze potential polyP-dependent differences in macromolecular damage using IbpA-msfGFP-
373 expressing WT and Δ*ppk* cells. *E. coli* produces polyP in response to AGXX®394C but not to Tob
374 (**Supplementary Fig. 4A-B**). IbpA-msfGFP-expressing WT and Δ*ppk* cells were exposed to a
375 combination of 10 µg/mL AGXX®394C and 0.2 µg/mL Tob for 1 hour, which is a combination
376 of AGXX®394C and Tob concentrations that resulted in the highest IbpA-msfGFP expression in
377 Δ*ppk* (**Supplementary Fig. 4B-D**). Confocal microscopy showed that IbpA-msfGFP foci in
378 untreated WT and Δ*ppk* cells were comparable with 12% and 6% of all cells, respectively (**Fig.
379 6D-E**). While in WT cells the combined treatment caused IbpA-msfGFP foci formation in ~20%
380 of the cells, foci were counted in ~85% of Δ*ppk* cells (**Fig. 6D-E**). The activation of the SOS
381 response in bacteria undergoing DNA damage has been shown to block cell division, leading to
382 abnormal growth and filamentation (38, 45). We quantified cell filamentation in AGXX®394C
383 /Tob-treated WT and Δ*ppk* cells, which was ~3-times higher in cells lacking polyP, indicating that
384 DNA damage in polyP-deficient cells is more pronounced (**Fig. 6F**). Flow cytometry analysis
385 further confirmed that AGXX®394C/Tob-induced IbpA-msfGFP expression was much more
386 prominent in polyP-deficient cells (**Fig. 6G-H**). Taken together, our data point towards a critical
387 role for polyP in protecting UPEC from the deleterious effects of AGXX®/aminoglycoside-
388 induced macromolecular damage.
389

390 **DISCUSSION**

391 **AGXX®/aminoglycoside combinations exhibit broad-spectrum antimicrobial activity.** The
392 emergence of antibiotic resistance is escalating global public health concern. Given the lack of
393 new antimicrobials in the industrial pipeline, novel approaches are desperately needed to combat
394 bacterial pathogens that are otherwise difficult to eradicate. The threat of growing antimicrobial
395 resistance is further compounded by the ability of many pathogenic bacteria to form protected
396 multicellular biofilm communities. Not only does biofilm formation offer defense from
397 antimicrobials, which struggle to diffuse through the extracellular matrix shield, they also enhance
398 the opportunity for the passage of antimicrobial resistance genes between bacterial species via
399 horizontal gene transfer. Biofilm-mediated resistance, along with antimicrobial resistance, is
400 especially problematic in relation to device-associated nosocomial infections (i.e., catheter-
401 associated UTIs, intravenous catheter infection, medical implant-associated infections). To try
402 and combat these ever evolving threats, a promising area of research has been directed towards the

403 use of compounds that increase the efficacy of antibiotics by targeting metabolic processes and/or
404 cellular networks (46). Compounds with synergistic effects have been reported for
405 aminoglycosides (1), as well as beta-lactams (47–49), rifampicin (50), and macrolides (51). Here,
406 we report on the synergistic interaction between aminoglycosides and AGXX®, a ROS-generating
407 surface coating comprised of the two transition metals Ag and Ru. The antimicrobial activity of
408 different AGXX® formulations is attributed to their specific coating composition, including the
409 silver-ruthenium ratio, particle size, and production procedure (27). Silver and silver-containing
410 derivates such as silver nanoparticles have been previously reported as potent enhancers of
411 aminoglycoside activity in *P. aeruginosa* and other pathogenic bacteria (19, 52–55). These
412 synergies have been shown to have especially meaningful potential clinical implications, with their
413 use as antimicrobial surface-coatings on catheters and other medical implants (56). Moreover,
414 silver derivatives such as silver sulfadiazine are currently used in topical applications, as a standard
415 for treating and preventing wound infections, despite being associated with side effects such as
416 allergic reactions to the sulfadiazine moiety (57). Intriguingly, AGXX® has been shown to be
417 significantly more potent than classical silver and silver sulfadiazine (58), is predicted to cause
418 minimal toxicity to human cells due to minimal release of Ag even after several weeks (25, 28),
419 and, to our knowledge, antimicrobial resistance to AGXX® has not been reported yet. Combined,
420 these characteristics make AGXX® potentially well-suited for applications as a novel
421 antimicrobial surface coating for medical devices.
422
423 Following up on from our previous study, showing that AGXX® potentiates the bactericidal
424 activities of aminoglycosides in the Gram-negative opportunistic pathogen *P. aeruginosa* (26), we
425 now provide evidence that the activity of AGXX®/aminoglycoside co-treatments extends to other
426 ESKAPEE pathogens including MDR-resistant *K. pneumoniae*, *A. baumannii*, *S. aureus*, and
427 UPEC strains (**Fig. 1; Fig. 2A**). Our killing assays revealed that regardless of the strain tested,
428 exposure to combinatorial AGXX®/aminoglycoside treatment, rapidly causes a 3- to 5-log
429 reduction in bacterial survival compared to the individual treatments. Most importantly,
430 AGXX®/aminoglycoside co-treatments reduced antibiotic concentrations required for efficient
431 killing of clinical ESKAPEE pathogen isolates, which are characterized by high gentamicin and
432 tobramycin resistance, by between 8-fold and 16-fold respectively (**Fig. 1; Supplementary Fig.
433 S1**). This may minimize the risk and/or severity of side effects caused by the antibiotic, and

434 possibly override/delay resistance development (59). These data are consistent with our previous
435 observation that AGXX® re-sensitizes an intrinsically resistant *P. aeruginosa* strain to sub-MIC
436 concentrations of kanamycin (26), and underscore the broad-spectrum antimicrobial potential of
437 AGXX®.
438
439 **The synergy between AGXX® and aminoglycosides is based on the induction of severe**
440 **oxidative stress that impairs cellular redox homeostasis.** Our current study further demonstrates
441 that ROS accumulation is the central mechanism underlying the synergistic interaction between
442 AGXX® and aminoglycoside antibiotics. Consistent with our previous observation in *P.*
443 *aeruginosa* (26), fluorescence-based assays in UPEC revealed that AGXX®/aminoglycoside co-
444 treatments induce a ~13-fold increase in intracellular ROS levels compared to individual
445 treatments alone (**Fig. 2**). These elevated ROS levels were tightly linked to the induction of
446 canonical stress response pathways, such as the transcriptional upregulation of *ibpA*, which
447 encodes a small heat-shock protein involved in proteostasis; and *sulA*, a marker of SOS response
448 to DNA damage. Thus, our data point towards significant proteotoxic and genotoxic challenges
449 that AGXX®/aminoglycoside combinations impose on UPEC, likely exceeding a threshold that a
450 functional redox homeostasis can buffer. Flow cytometry and confocal microscopy further
451 demonstrated that AGXX®/Tob co-treatment induces IbpA-protein foci development to levels
452 comparable to bacteria under heat-shock (**Fig. 3**). The combinatorial treatment also produced
453 substantial protein aggregation, which was detected in ~80% of cells. These observations are
454 consistent with established models in which aminoglycosides promote mistranslation and the
455 accumulation of misfolded proteins (10), while AGXX® independently induces oxidative protein
456 damage through thiol oxidation leading to widespread protein aggregation (22, 27, 60). As a result,
457 expression of molecular chaperones and proteases is highly upregulated in AGXX®-stressed
458 bacteria, as previously shown in several independent transcriptome studies (21–24, 27).
459
460 AGXX® has recently been shown to induce detectable DNA double-strand breaks in a ROS-
461 dependent manner, when applied in sufficiently-high yet still sub-lethal concentrations (27). In our
462 present study, AGXX®/Tob co-treated cells were characterized by markedly exacerbated DNA
463 damage, as indicated by the development of Gam-sfGFP foci within the cells (**Fig. 4**). Gam is a
464 bacteriophage protein that binds to sites of double-strand DNA breaks (41). While

465 aminoglycosides specifically target protein translation, it has been reported that kanamycin can
466 damage DNA bases, which likely occurs indirectly as a result of ROS generation (61). We did not
467 observe significant Gam-sfGFP foci formation when cells were treated with AGXX® or
468 tobramycin alone, like due to the low concentrations of each stressor. Strikingly, the co-treatment
469 of AGXX®/Tob significantly amplified the genotoxic effects, with ~50% of the treated cells
470 displaying Gam-GFP foci, and ~85% of those cells showing multiple foci. This suggests that the
471 combinatorial treatment with AGXX®/Tob, significantly enhances the DNA damaging ability of
472 AGXX® in UPEC.
473
474 We further demonstrate that ROS are not merely a byproduct of but are the driver of
475 AGXX®/aminoglycoside toxicity. We found that pretreatment with the antioxidant thiourea
476 abolished AGXX®/Tob-induced ROS accumulation, restored bacterial survival to levels similar
477 to untreated bacteria, and suppressed IbpA-protein foci formation and protein aggregation (**Fig.**
478 **5**). This data therefore establishes oxidative imbalance as the initiating event that links AGXX®
479 exposure to enhanced aminoglycoside efficacy. This aligns with ROS-dependent models of
480 aminoglycoside killing (5, 26, 62) and reconciles previous controversies (7, 52) by demonstrating
481 that ROS become critical when aminoglycoside stress is amplified by a redox-active compound.
482 Together, these ROS-driven insults overwhelm bacterial macromolecules, providing a mechanistic
483 explanation for the pronounced bactericidal synergy of AGXX® with aminoglycosides.
484
485 **Bacteria produce polyphosphate to counter AGXX®/aminoglycoside toxicity.** Providing
486 further evidence to support this ROS-driven bactericidal synergy of AGXX® with
487 aminoglycosides, we found that UPEC protect themselves from this toxicity through
488 polyphosphate (polyP) (**Fig. 6, Supplementary Fig. S4**). Gram-negative bacteria have long been
489 known to produce polyP as a stress defense strategy to counter host defense mechanisms (32, 33,
490 63–65). In addition to being involved in various biological processes, including biofilm formation
491 (66, 67), motility (68), virulence factor production (69, 70), and host colonization (66, 69, 71),
492 polyP has also been identified as a potent chemical chaperone that protects bacteria from
493 proteotoxic stress (43, 44, 72, 73). Here, we demonstrate a significant increase in polyP production
494 when cells are exposed to AGXX® **(Fig. S4)**. This is consistent with a previous report, which also
495 showed that Δ*ppk* cells were highly sensitive towards silver nitrate and that the transcriptome of

496 AGXX-treated UPEC cells showed signs of silver exposure (27). While the deletion of *ppk1*, the
497 gene responsible for polyP production, has been associated with increased susceptibility of *E. coli*
498 and *P. aeruginosa* towards aminoglycoside and carbapenem antibiotics (74, 75), we did not detect
499 a significant induction in polyP production in Tob-treated cells (**Fig. S4**). Whether the activation
500 of polyP production is in response toAGXX®/aminoglycosides-generated ROS, or potentially to
501 silver ions that are released from the AGXX® formulation remains unclear. We conclude that
502 PolyP, likely induced by ROS accumulation, acts as a chemical chaperone to protect from the
503 proteotoxic effects of AGXX®/Tob, and propose that both IbpA expression and polyP production
504 are important for a stringent defense. This may explain why, compared to Δ*ppk* strains, IbpA-
505 msfGFP expression is substantially reduced and IbpA-msfGFP foci are present in much fewer cells
506 in the polyP-producing WT strain. In the absence of polyP, cells depend primarily on IbpA-
507 mediated chaperone activity to counter AGXX®/Tob-mediated proteotoxic stress. However, this
508 compensatory mechanism is insufficient to prevent widespread damage, and our data highlights
509 the critical role of polyP in protecting bacterial cells from redox-induced proteome disruptions.
510
511 Collectively, our study positions AGXX® as a dual-function antimicrobial that potentiates
512 aminoglycoside effects on Gram-negative pathogens, by intensifying ROS-mediated proteotoxic
513 and genotoxic stress. By driving bacterial stress responses beyond recoverable thresholds,
514 AGXX® potentiates the efficacy of aminoglycoside exposure with detrimental effects on bacterial
515 viability. More broadly, our work highlights controlled redox stress as a rational strategy for
516 antibiotic potentiation and provides a mechanistic framework for the development of ROS-based
517 antimicrobial adjuvants.
518

519 **MATERIALS AND METHODS**

520 **Bacterial strains and growth conditions.** All strains, plasmids, and oligonucleotides used in this
521 study are listed in **Supplementary Table 2**. Unless stated otherwise, overnight cultures were
522 grown aerobically in Luria-Bertani (LB) broth (Millipore Sigma) at 37°C with shaking at 300 rpm
523 for 16-20 hours. For subsequent experiments, overnight cultures were diluted into 3-(N-
524 morpholino) propanesulfonic acid minimal medium supplemented with 0.2% glucose, 1.32 mM
525 K_2HPO_4, and 10 μM thiamine (76), or in artificial urine media (AUM) (29), and incubated at 37°C
526 under shaking conditions.

527

528 **Preparation of artificial urine media (AUM).** AUM was prepared as previously described (29).
529 The final concentrations of the components were as follows: 78.5 mM sodium chloride, 9 mM
530 sodium sulfate, 2.2 mM sodium citrate dihydrate, 0.1 mM sodium oxalate, 3.6 mM potassium
531 dihydrogen phosphate, 21.5 mM potassium chloride, 3 g/L tryptic soy broth, 3 mM calcium
532 chloride, 2 mM magnesium chloride, 15 mM ammonium chloride, 6 mM creatinine, and 200 mM
533 urea (pH 6.3). The AUM was freshly prepared every 7 to 10 days.

534

535 **Preparation of AGXX® formulations.** All AGXX® formulations used in this study were
536 developed and supplied by Largentec GmbH (Berlin, Germany). AGXX®394C and AGXX®720C
537 microparticles used in this study were made from silver powders on cellulose with a particle size
538 between 1.5 to 2.5 µm (MaTeck, Germany). The silver-ruthenium complex was realized by
539 Largentec proprietary electrochemical deposition processes.

540

541 **Time killing assay of clinical isolates.** Overnight cultures were diluted ~20-fold into MHB by
542 normalizing cultures to an optical density at 600 nm (OD_{600}) = 0.1 in a six-well sterile cell culture
543 plate. Samples were then treated with sublethal concentrations of AGXX®720C and Gm or Tob
544 individually or in combination. Cell culture plates incubated at 37°C for four hours at 150 rpm
545 under aerobic conditions. Cells were collected at indicated time points, serially diluted in
546 phosphate-buffered saline (PBS, pH 7.4), plated on LB agar and incubated at 37°C for 20 hours to
547 quantify surviving colonies.

548

549 **Bacterial survival assays.** Overnight cultures of UPEC strains CFT073 or CFT073Δ*ppk* were
550 diluted 50-fold into the indicated media to an initial OD_{600} ~ 0.08 and incubated until reaching an
551 OD_{600} = 0.3. Cultures were then transferred to sterile 125 mL flasks and exposed to sublethal
552 concentrations of AGXX®, the indicated aminoglycosides, or the combination thereof. If
553 indicated, cultures were pretreated with 70 mM thiourea for 60 minutes prior to AGXX® and/or
554 aminoglycoside exposure. After 1 hour, aliquots were serially diluted in PBS, plated on LB agar,
555 and incubated overnight at 37°C under shaking conditions for colony-forming unit (CFU) counts.

556

557 **Checkerboard Assay.** Checkerboard assays were performed as previously described (77), with
558 slight modifications. 100x stock solutions of the indicated aminoglycoside antibiotics were serially
559 diluted and added to the respective wells of 12-well plates, while the concentration of
560 AGXX®720C was held constant across wells. Exponentially growing UPEC CFT073 cultures in
561 MOPSg minimal media were adjusted to an initial OD_{600} of approximately 0.05 and added to each
562 well. Plates were incubated at 37°C with shaking for 16–18 hours. OD_{600} was subsequently
563 measured to assess bacterial growth.
564
565 **Intracellular ROS quantification.** Intracellular ROS levels were quantified using the redox-
566 sensitive dye 2′,7′-dichlorodihydrofluorescein diacetate (H_2DCFDA) (Thermo Fisher Scientific).
567 Exponentially growing cultures of CFT073 and CFT073Δ*ppk* were left untreated or treated with
568 the indicated concentrations of AGXX®394C, Tob, or their combination for 1 hour. Duplicate
569 samples were then collected, washed once with pre-warmed PBS, normalized to an OD_{600} ~1.0 in
570 prewarmed PBS containing 10 μM H_2DCFDA, incubated in the dark at 37°C for 30 minutes,
571 washed again with PBS before DCF fluorescence was measured at excitation/emission
572 wavelengths of 485/535 nm in a Tecan Infinite 200 plate reader. If indicated, cells were incubated
573 with 70 mM of the ROS quencher thiourea prior to stress treatments.
574
575 **Gene expression analysis by qRT-PCR.** Overnight cultures of CFT073 were diluted into MOPSg
576 medium to an OD_{600} ~ 0.08 and grown to mid-log phase (OD_{600} ~ 0.3). Cultures were either left
577 untreated or treated with 30 μg/ml AGXX®394C, 0.5 μg/ml Tob, or their combination. Following
578 10 mins of incubation, transcription was halted by the addition of ice-cold methanol. Total RNA
579 was extracted from at least three biological replicates using a commercial RNA extraction kit
580 (Macherey-Nagel), residual genomic DNA was removed with the TURBO DNA-free kit (Thermo
581 Scientific), and mRNA reverse transcribed into cDNA using the PrimeScript cDNA synthesis kit
582 (Takara). qRT-PCRs were performed using manufacturer protocols (Alkali Scientific) with gene-
583 specific primers (e.g., *ibpA, sulA*, and *rrsD*). Gene expression was normalized to *rrsD*, and relative
584 transcript levels were determined using the $2^{-\Delta\Delta CT}$ method (78).
585
586 **IbpA-msfGFP expression by flow cytometry.** Overnight cultures of strains MG1655::*ibpA-*
587 *msfGFP* and MG1655Δ*ppk::ibpA-msfGFP* were diluted into fresh MOPSg medium to an OD_{600}

588 ~0.01 and grown to mid-log phase (OD_{600} ~ 0.3). Prior to cultures reaching mid-log phase, cells
589 were then left untreated or pretreated with 70 mM thiourea before the indicated concentrations of
590 AGXX®394C, Tob, or their combination were added for 1 hour. Cells exposed to 50°C for 60
591 mins served as positive controls. For flow cytometry analysis of IbpA-sfGFP expression, samples
592 were normalized to an OD_{600} of 0.05 in PBS (pH 7.4) and analyzed on a BD FACS Melody
593 cytometer via the FITC channel, recording at least 10,000 events per sample. Data were analyzed
594 with FCSalyzer.
595
596 **IbpA-msfGFP binding to protein aggregates *in vivo*.** Overnight cultures of strains
597 MG1655::*ibpA-msfGFP* and MG1655Δ*ppk::ibpA-msfGFP* were diluted into fresh MOPSg
598 medium to an OD_{600} ~ 0.01 and grown to mid-log phase (OD_{600} ~ 0.3). Prior to cultures reaching
599 mid-log phase, cells were then left untreated or pretreated with 70 mM thiourea before the
600 indicated concentrations of AGXX®394C, Tob, or their combination were added for 1 hour. Cells
601 exposed to 50°C for 60 min served as positive controls. For visualization of IbpA-sfGFP-bound
602 protein aggregates, cells were washed twice in PBS, stained with 5 µg/mL DAPI and 5 µg/mL
603 FM4-64 in the dark for 15 minutes, washed again, and mounted on 1% agarose pads. Fluorescence
604 microscopy was performed using a Leica SP8 confocal system with a DMi8 CS inverted
605 microscope. At least 500 cells across all replicates were blindly quantified.
606
607 **Gam-GFP binding to DNA double-strand breaks.** Strain MG1655::*gam-gfp* was grown
608 overnight in LB supplemented with 200 ng/mL doxycycline to induce Gam-GFP expression. Cells
609 were diluted into doxycycline-containing MOPSg medium to an OD_{600} ~0.08 and grown to mid-
610 log phase (OD_{600} ~ 0.3), and treated with the indicated concentrations of AGXX®394C, Tob, or
611 their combination. Addition of ciprofloxacin was used as a positive control for DNA damage.
612 Following 3 hours of treatment, cells were washed twice, resuspended in PBS, stained with 5
613 µg/mL DAPI and 5 µg/mL FM4-64 in the dark for 15 minutes, washed again prior to resuspension
614 in PBS. Samples were imaged on 1% agarose gel pads using a Leica SP8 confocal system, which
615 is equipped with a DMi8 CS inverted microscope. At least 500 cells across all replicates were
616 counted blindly.
617

618 **Construction of in-frame gene deletions in *E. coli* cells expressing IbpA-sfGFP**. An in-frame
619 *ppk* deletion mutant was constructed using the lambda red-mediated site-specific recombination
620 (79). In brief, the *ppk* gene in *E. coli* MG1655-*ibpA*-msfGFP was replaced by a chloramphenicol
621 resistance cassette, which was subsequently resolved using pCP20 to yield the nonpolar in-frame
622 deleted strain MG1655-*ibpA*-msfGFPΔ*ppk*. The chromosomal mutation was verified by PCR.
623
624 **PolyP extraction and quantification.** Intracellular polyP levels were extracted as previously
625 described (70, 80) with minor modifications and quantified with DAPI. Mid-log phase cultures of
626 the IbpA-msfGFP-expressing *E. coli* WT and Δ*ppk*1 strains were grown in MOPSg at 37°C under
627 aerobic conditions and exposed to the indicated concentrations of Tob or AGXX®394C for 1 h.
628 Following treatment, cultures were normalized to an OD_{600} of 0.3, and 1mL aliquots were
629 harvested by centrifugation at 8,000 ×g, 5 min, 4°C. Cell pellets were resuspended in 200 µL
630 guanidinium isothiocyanate (GITC) lysis buffer and incubated at 95°C for 10 min to release
631 intracellular polyP. A 50 µL aliquot of the crude lysate was reserved for total protein determination
632 using the Bradford assay. The remaining lysate was mixed with 95% ethanol and applied to silica
633 membrane EconoSpin columns (Epoch Life Science) for polyP purification. Columns were
634 washed twice with 5 mM Tris-HCl (pH 7.5), and polyP was eluted with 50 mM Tris-HCl (pH 8.0).
635 Eluted polyP was mixed with 25 µM DAPI, incubated in the dark for 10 min, and fluorescence
636 was measured at Exc./em. wavelengths of 420/550 nm, which preferentially detects DAPI–polyP
637 complexes. DAPI in elution buffer was deducted as buffer control. Further, the background was
638 determined by treating the purified polyP samples with 1 mg Ppx for an hour prior to staining in
639 DAPI. PolyP concentrations were then extrapolated using a sodium polyP standard curve that was
640 prepared in 50mM Tris HCl, pH 8.0.
641
642 **Growth curve-based assays.** Overnight cultures of CFT073 and CFT073Δ*ppk* were diluted ~50-
643 fold into MOPSg media, grown to early stationary phase, diluted again into fresh MOPSg to an
644 OD_{600} = 0.02, and incubated in a Tecan Infinite 200 plate reader with or without the indicated
645 concentrations of AGXX®394C, Tob, or their combination. Absorbance at 600 nm was measured
646 every 10 minutes for 16 hours.
647
648 **Statistical analyses.** All statistical analyses were performed in GraphPad Prism version 8.0.

649 **ACKNOWLEDGEMENTS**

650 This work was supported by the NIAID grant 1R03AI174033-01A1 (to J.-U. D.). We thank
651 members of the Dahl and Floyd labs for discussion and feedback. The Largentec GmbH team is
652 acknowledged for providing the different AGXX® formulations and for helpful discussions, Susan
653 Rosenberg (Baylor College of Medicine) and Abram Aertsen (KU Leuven) for strains expressing
654 Gam-GFP and IbpA-msfGFP, respectively.

REFERENCES

1. Tawiah PO, Sultana S, Dahl J-U. 2025. Unlocking Enhanced Efficacy of Aminoglycoside Antibiotics Against Pseudomonas aeruginosa. Microb Biotechnol 18:e70174.

2. Saika T, Hasegawa M, Kobayashi I, Nishida M. 1998. [Ionic binding of 3H-gentamicin and short-term bactericidal activity of gentamicin against Pseudomonas aeruginosa isolates differing in lipopolysaccharide structure]. Kansenshogaku Zasshi 72:97–104.

3. Martin NL, Beveridge TJ. 1986. Gentamicin interaction with Pseudomonas aeruginosa cell envelope. Antimicrob Agents Chemother 29:1079–1087.

4. Joshi T, Voo ZX, Graham B, Spiccia L, Martin LL. 2015. Real-time examination of aminoglycoside activity towards bacterial mimetic membranes using Quartz Crystal Microbalance with Dissipation monitoring (QCM-D). Biochim Biophys Acta 1848:385–391.

5. Kohanski MA, Dwyer DJ, Wierzbowski J, Cottarel G, Collins JJ. 2008. Mistranslation of membrane proteins and two-component system activation trigger aminoglycoside-mediated oxidative stress and cell death. Cell 135:679–690.

6. Davis BD, Chen LL, Tai PC. 1986. Misread protein creates membrane channels: an essential step in the bactericidal action of aminoglycosides. Proc Natl Acad Sci U S A 83:6164–6168.

7. Liu Y, Imlay JA. 2013. Cell death from antibiotics without the involvement of reactive oxygen species. Science 339:1210–1213.

8. Dwyer DJ, Belenky PA, Yang JH, MacDonald IC, Martell JD, Takahashi N, Chan CTY, Lobritz MA, Braff D, Schwarz EG, Ye JD, Pati M, Vercruysse M, Ralifo PS, Allison KR, Khalil AS, Ting AY, Walker GC, Collins JJ. 2014. Antibiotics induce redox-related physiological alterations as part of their lethality. Proc Natl Acad Sci U S A 111:E2100-2109.

9. Ramirez MS, Tolmasky ME. 2010. Aminoglycoside modifying enzymes. Drug Resist Updat 13:151–171.

10. Ezraty B, Vergnes A, Banzhaf M, Duverger Y, Huguenot A, Brochado AR, Su S-Y, Espinosa L, Loiseau L, Py B, Typas A, Barras F. 2013. Fe-S Cluster Biosynthesis Controls Uptake of Aminoglycosides in a ROS-Less Death Pathway. Science 340:1583–1587.

11. Kaper JB, Nataro JP, Mobley HLT. 2004. Pathogenic Escherichia coli. Nat Rev Microbiol 2:123–140.

12. Klein RD, Hultgren SJ. 2020. Urinary tract infections: microbial pathogenesis, host-pathogen interactions and new treatment strategies. Nat Rev Microbiol 18:211–226.

13. Flores-Mireles AL, Walker JN, Caparon M, Hultgren SJ. 2015. Urinary tract infections: epidemiology, mechanisms of infection and treatment options. Nat Rev Microbiol 13:269–284.

14. Saleem Z, Godman B, Hassali MA, Hashmi FK, Azhar F, Rehman IU. 2019. Point prevalence surveys of health-care-associated infections: a systematic review. Pathogens and Global Health 113:191–205.

15. Andersen MJ, Flores-Mireles AL. 2020. Urinary Catheter Coating Modifications: The Race against Catheter-Associated Infections. 1. Coatings 10:23.

16. Timm MR, Russell SK, Hultgren SJ. 2024. Urinary tract infections: pathogenesis, host susceptibility and emerging therapeutics. Nat Rev Microbiol 1–15.

17. Lansdown ABG. 2010. A pharmacological and toxicological profile of silver as an antimicrobial agent in medical devices. Adv Pharmacol Sci 2010:910686.

18. Grass G, Rensing C, Solioz M. 2011. Metallic copper as an antimicrobial surface. Appl Environ Microbiol 77:1541–1547.

19. Barras F, Aussel L, Ezraty B. 2018. Silver and Antibiotic, New Facts to an Old Story. Antibiotics 7:79.

20. Nolan LK, Li G, Logue CM. 2015. Origin and Dissemination of Antimicrobial Resistance among Uropathogenic Escherichia coli. Microbiol Spectr 3.

21. Sobisch L-Y, Rogowski KM, Fuchs J, Schmieder W, Vaishampayan A, Oles P, Novikova N, Grohmann E. 2019. Biofilm Forming Antibiotic Resistant Gram-Positive Pathogens Isolated From Surfaces on the International Space Station. Front Microbiol 10:543.

22. Loi VV, Busche T, Preuß T, Kalinowski J, Bernhardt J, Antelmann H. 2018. The AGXX® Antimicrobial Coating Causes a Thiol-Specific Oxidative Stress Response and Protein S-bacillithiolation in Staphylococcus aureus. Front Microbiol 9:3037.

23. Clauss-Lendzian E, Vaishampayan A, de Jong A, Landau U, Meyer C, Kok J, Grohmann E. 2018. Stress response of a clinical Enterococcus faecalis isolate subjected to a novel antimicrobial surface coating. Microbiological Research 207:53–64.

24. Vaishampayan A, de Jong A, Wight DJ, Kok J, Grohmann E. 2018. A Novel Antimicrobial Coating Represses Biofilm and Virulence-Related Genes in Methicillin-Resistant Staphylococcus aureus. Front Microbiol 9:221.

25. Guridi A, Diederich A-K, Aguila-Arcos S, Garcia-Moreno M, Blasi R, Broszat M, Schmieder W, Clauss-Lendzian E, Sakinc-Gueler T, Andrade R, Alkorta I, Meyer C, Landau U, Grohmann E. 2015. New antimicrobial contact catalyst killing antibiotic resistant clinical and waterborne pathogens. Mater Sci Eng C Mater Biol Appl 50:1–11.

26. Donkor GY, Anderson GM, Stadler M, Tawiah PO, Orellano CD, Edwards KA, Dahl J-U. 2023. A novel ruthenium-silver based antimicrobial potentiates aminoglycoside activity against Pseudomonas aeruginosa. mSphere e0019023.

27. Tawiah PO, Gaessler LF, Anderson GM, Oladokun EP, Dahl J-U. 2025. A novel silver-ruthenium-based antimicrobial kills Gram-negative bacteria through oxidative stress-induced macromolecular damage. mSphere 10:e0001725.

28. Linzner N, Antelmann H. 2021. The Antimicrobial Activity of the AGXX® Surface Coating Requires a Small Particle Size to Efficiently Kill Staphylococcus aureus. Front Microbiol 12:731564.

29. Brooks T, Keevil CW. 1997. A simple artificial urine for the growth of urinary pathogens. Letters in Applied Microbiology 24:203–206.

30. Ezraty B, Gennaris A, Barras F, Collet J-F. 2017. Oxidative stress, protein damage and repair in bacteria. Nat Rev Microbiol 15:385–396.

31. Cooke MS, Evans MD, Dizdaroglu M, Lunec J. 2003. Oxidative DNA damage: mechanisms, mutation, and disease. The FASEB Journal 17:1195–1214.

32. Dahl J-U, Gray MJ, Jakob U. 2015. Protein Quality Control under Oxidative Stress Conditions. Journal of Molecular Biology 427:1549–1563.

33. Sultana S, Foti A, Dahl J-U. 2020. Bacterial Defense Systems against the Neutrophilic Oxidant Hypochlorous Acid. Infect Immun 88:e00964-19.

34. Brand C, Newton-Foot M, Grobbelaar M, Whitelaw A. 2025. Antibiotic-induced stress responses in Gram-negative bacteria and their role in antibiotic resistance. J Antimicrob Chemother 80:1165–1184.

35. Sultana S, Dahl J-U. 2023. A Year at the Forefront of Bacterial Defense Systems Against Neutrophilic Oxidants. Biol Open 12:bio059809.

36. Sen A, Imlay JA. 2021. How Microbes Defend Themselves From Incoming Hydrogen Peroxide. Front Immunol 12:667343.

37. Miwa T, Taguchi H. 2025. Revival of the Escherichia coli heat shock response after two decades with a small Hsp in a critical but distinct act. Biol Chem 406:29–33.

38. Mukherjee A, Cao C, Lutkenhaus J. 1998. Inhibition of FtsZ polymerization by SulA, an inhibitor of septation in *Escherichia coli*. Proc Natl Acad Sci USA 95:2885–2890.

39. Ratajczak E, Zietkiewicz S, Liberek K. 2009. Distinct activities of Escherichia coli small heat shock proteins IbpA and IbpB promote efficient protein disaggregation. J Mol Biol 386:178–189.

40. Govers SK, Mortier J, Adam A, Aertsen A. 2018. Protein aggregates encode epigenetic memory of stressful encounters in individual Escherichia coli cells. PLoS Biol 16:e2003853.

41. Shee C, Cox BD, Gu F, Luengas EM, Joshi MC, Chiu L-Y, Magnan D, Halliday JA, Frisch RL, Gibson JL, Nehring RB, Do HG, Hernandez M, Li L, Herman C, Hastings PJ, Bates D, Harris RS, Miller KM, Rosenberg SM. 2013. Engineered proteins detect spontaneous DNA breakage in human and bacterial cells. Elife 2:e01222.

42. Bryan LE, Kwan S. 1983. Roles of ribosomal binding, membrane potential, and electron transport in bacterial uptake of streptomycin and gentamicin. Antimicrobial Agents and Chemotherapy 23:835–845.

43. Groitl B, Dahl J-U, Schroeder JW, Jakob U. 2017. *Pseudomonas aeruginosa* defense systems against microbicidal oxidants: Defense systems against microbicidal oxidants. Molecular Microbiology 106:335–350.

44. Gray MJ, Wholey W-Y, Wagner NO, Cremers CM, Mueller-Schickert A, Hock NT, Krieger AG, Smith EM, Bender RA, Bardwell JCA, Jakob U. 2014. Polyphosphate Is a Primordial Chaperone. Molecular Cell 53:689–699.

45. Kreuzer KN. 2013. DNA Damage Responses in Prokaryotes: Regulating Gene Expression, Modulating Growth Patterns, and Manipulating Replication Forks. Cold Spring Harbor Perspectives in Biology 5:a012674–a012674.

46. Wright GD. 2016. Antibiotic Adjuvants: Rescuing Antibiotics from Resistance. Trends in Microbiology 24:862–871.

47. Bilal H, Bergen PJ, Kim TH, Chung SE, Peleg AY, Oliver A, Nation RL, Landersdorfer CB. 2019. Synergistic Meropenem-Tobramycin Combination Dosage Regimens against Clinical Hypermutable Pseudomonas aeruginosa at Simulated Epithelial Lining Fluid Concentrations in a Dynamic Biofilm Model. Antimicrob Agents Chemother 63:e01293-19.

48. Giamarellou H, Zissis NP, Tagari G, Bouzos J. 1984. In vitro synergistic activities of aminoglycosides and new beta-lactams against multiresistant Pseudomonas aeruginosa. Antimicrob Agents Chemother 25:534–536.

49. Pankuch GA, Lin G, Kubo A, Armstrong ES, Appelbaum PC, Kosowska-Shick K. 2011. Activity of ACHN-490 Tested Alone and in Combination with Other Agents against Pseudomonas aeruginosa. Antimicrobial Agents and Chemotherapy 55:2463–2465.

50. Poole K, Gilmour C, Farha MA, Mullen E, Lau CH-F, Brown ED. 2016. Potentiation of Aminoglycoside Activity in Pseudomonas aeruginosa by Targeting the AmgRS Envelope Stress-Responsive Two-Component System. Antimicrob Agents Chemother 60:3509–3518.

51. Tré-Hardy M, Nagant C, El Manssouri N, Vanderbist F, Traore H, Vaneechoutte M, Dehaye J-P. 2010. Efficacy of the combination of tobramycin and a macrolide in an in vitro

Pseudomonas aeruginosa mature biofilm model. Antimicrob Agents Chemother 54:4409–4415.

52. Herisse M, Duverger Y, Martin-Verstraete I, Barras F, Ezraty B. 2017. Silver potentiates aminoglycoside toxicity by enhancing their uptake. Mol Microbiol 105:115–126.

53. Morones-Ramirez JR, Winkler JA, Spina CS, Collins JJ. 2013. Silver enhances antibiotic activity against gram-negative bacteria. Sci Transl Med 5:190ra81.

54. Dove AS, Dzurny DI, Dees WR, Qin N, Nunez Rodriguez CC, Alt LA, Ellward GL, Best JA, Rudawski NG, Fujii K, Czyż DM. 2022. Silver nanoparticles enhance the efficacy of aminoglycosides against antibiotic-resistant bacteria. Front Microbiol 13:1064095.

55. Habash MB, Goodyear MC, Park AJ, Surette MD, Vis EC, Harris RJ, Khursigara CM. 2017. Potentiation of Tobramycin by Silver Nanoparticles against Pseudomonas aeruginosa Biofilms. Antimicrob Agents Chemother 61:e00415-17.

56. Lansdown ABG. 2010. A pharmacological and toxicological profile of silver as an antimicrobial agent in medical devices. Adv Pharmacol Sci 2010:910686.

57. Fuller FW. 2009. The side effects of silver sulfadiazine. J Burn Care Res 30:464–470.

58. Carr HS, Wlodkowski TJ, Rosenkranz HS. 1973. Silver sulfadiazine: in vitro antibacterial activity. Antimicrob Agents Chemother 4:585–587.

59. Rosenberg CR, Fang X, Allison KR. 2020. Potentiating aminoglycoside antibiotics to reduce their toxic side effects. PLoS One 15:e0237948.

60. Sultana S, Anderson GM, Hoffmann KP, Dahl J-U. 2021. Extraction and Visualization of Protein Aggregates after Treatment of Escherichia coli with a Proteotoxic Stressor. JoVE (Journal of Visualized Experiments) e62628.

61. Kang TM, Yuan J, Nguyen A, Becket E, Yang H, Miller JH. 2012. The Aminoglycoside Antibiotic Kanamycin Damages DNA Bases in Escherichia coli: Caffeine Potentiates the DNA-Damaging Effects of Kanamycin while Suppressing Cell Killing by Ciprofloxacin in Escherichia coli and Bacillus anthracis. Antimicrob Agents Chemother 56:3216–3223.

62. Kohanski MA, Dwyer DJ, Hayete B, Lawrence CA, Collins JJ. 2007. A Common Mechanism of Cellular Death Induced by Bactericidal Antibiotics. Cell 130:797–810.

63. Rao NN, Gómez-García MR, Kornberg A. 2009. Inorganic Polyphosphate: Essential for Growth and Survival. Annu Rev Biochem 78:605–647.

64. Bowlin MQ, Gray MJ. 2021. Inorganic polyphosphate in host and microbe biology. Trends in Microbiology 29:1013–1023.

65. Gray MJ, Jakob U. 2015. Oxidative stress protection by polyphosphate—new roles for an old player. Current Opinion in Microbiology 24:1–6.

66. Rashid MH, Rumbaugh K, Passador L, Davies DG, Hamood AN, Iglewski BH, Kornberg A. 2000. Polyphosphate kinase is essential for biofilm development, quorum sensing, and virulence of Pseudomonas aeruginosa. Proceedings of the National Academy of Sciences 97:9636–9641.

67. Fraley CD, Rashid MH, Lee SSK, Gottschalk R, Harrison J, Wood PJ, Brown MRW, Kornberg A. 2007. A polyphosphate kinase 1 (ppk1) mutant of Pseudomonas aeruginosa exhibits multiple ultrastructural and functional defects. Proc Natl Acad Sci USA 104:3526–3531.

68. Rashid MH, Kornberg A. 2000. Inorganic polyphosphate is needed for swimming, swarming, and twitching motilities of Pseudomonas aeruginosa. Proceedings of the National Academy of Sciences 97:4885–4890.

69. Neville N, Roberge N, Ji X, Stephen P, Lu JL, Jia Z. 2021. A Dual-Specificity Inhibitor Targets Polyphosphate Kinase 1 and 2 Enzymes To Attenuate Virulence of Pseudomonas aeruginosa. mBio 12:e0059221.

70. Shah R, Narh JK, Urlaub M, Jankiewicz O, Johnson C, Livingston B, Dahl J-U. 2024. Pseudomonas aeruginosa kills Staphylococcus aureus in a polyphosphate-dependent manner. mSphere e0068624.

71. Dahl J-U, Gray MJ, Bazopoulou D, Beaufay F, Lempart J, Koenigsknecht MJ, Wang Y, Baker JR, Hasler WL, Young VB, Sun D, Jakob U. 2017. The anti-inflammatory drug mesalamine targets bacterial polyphosphate accumulation. Nat Microbiol 2:16267.

72. Yoo NG, Dogra S, Meinen BA, Tse E, Haefliger J, Southworth DR, Gray MJ, Dahl J-U, Jakob U. 2018. Polyphosphate Stabilizes Protein Unfolding Intermediates as Soluble Amyloid-like Oligomers. Journal of Molecular Biology 430:4195–4208.

73. Cremers CM, Knoefler D, Gates S, Martin N, Dahl J-U, Lempart J, Xie L, Chapman MR, Galvan V, Southworth DR, Jakob U. 2016. Polyphosphate: A Conserved Modifier of Amyloidogenic Processes. Molecular Cell 63:768–780.

74. Chen J, Su L, Wang X, Zhang T, Liu F, Chen H, Tan C. 2016. Polyphosphate Kinase Mediates Antibiotic Tolerance in Extraintestinal Pathogenic Escherichia coli PCN033. Front Microbiol 7.

75. Ortiz-Severín J, Varas M, Bravo-Toncio C, Guiliani N, Chávez FP. 2015. Multiple antibiotic susceptibility of polyphosphate kinase mutants (ppk1 and ppk2) from Pseudomonas aeruginosa PAO1 as revealed by global phenotypic analysis. Biol Res 48:22.

76. Neidhardt FC, Bloch PL, Smith DF. 1974. Culture medium for enterobacteria. J Bacteriol 119:736–747.

77. Canchola J, Donkor GYB, Tawiah PO, Fasawe A, Ayim E, Engelke MF, Dahl J-U. 2024. Alkyl Pyridinol Compounds Exhibit Antimicrobial Effects against Gram-Positive Bacteria. Antibiotics (Basel) 13:897.

78. Pfaffl MW. 2001. A new mathematical model for relative quantification in real-time RT-PCR. Nucleic Acids Res 29:e45.

79. Datsenko KA, Wanner BL. 2000. One-step inactivation of chromosomal genes in Escherichia coli K-12 using PCR products. Proceedings of the National Academy of Sciences 97:6640–6645.

80. Dahl J, Xie L, Jakob U. 2018. Extraction and Quantification of Polyphosphate (polyP) from Gram-negative Bacteria. BIO-PROTOCOL 8.